Hindawi
Advances in Materials Science and Engineering
Volume 2023, Article ID 5952072, 16 pages
https://doi.org/10.1155/2023/5952072

Research Article

Prediction of Mechanical Properties of Aluminium Alloy Strip Using the Extreme Learning Machine Model Optimized by the Gray Wolf Algorithm

Zhenqiang Xiong, Jiadong Li, Peng Zhao, and Yong Li

The State Key Laboratory of Rolling and Automation, Northeastern University, Shenyang 110819, China

Correspondence should be addressed to Jiadong Li; lijd@ral.neu.edu.cn

Received 21 September 2022; Revised 15 April 2023; Accepted 12 May 2023; Published 4 July 2023

Academic Editor: Alicia E. Ares

Mechanical properties are important indicators for evaluating the quality of strips. This paper proposes a mechanical performance prediction model based on the Gray Wolf Optimization (GWO) algorithm and the Extreme Learning Machine (ELM) algorithm. In the modeling process, GWO is used to determine the optimal weights and deviations of ELM and experiments are used to determine the model's key parameters. The model effectively avoids manual intervention and significantly improves aluminum alloy strips' mechanical property prediction accuracy. This paper uses processed data from the aluminum alloy production plant of Shandong Nanshan Aluminum Co., Ltd. as experimental data. When the prediction deviation is controlled within ±10%, the GWO-ELM model can achieve a correct rate of 100% for tensile strength, 97.5% for yield strength, and 77.5% for elongation on the test set. The RMSE of the tensile strength, yield strength, and elongation of the GWO-ELM model was 5.365, 11.881, and 1.268, respectively. The experimental results show that the GWO-ELM model has higher accuracy and stability in predicting aluminum alloy strips' tensile strength, yield strength, and elongation. The GWO-ELM model effectively avoids the defects of the traditional model. It has a special guiding significance for producing aluminum alloy strips.

1. Introduction

Among the many indicators of hot-rolled alloy products, mechanical properties, which are influenced by the complexity of processing parameters, are one of the important indicators of the quality of hot-rolled alloy products. Therefore, the mechanical properties of alloy products are valued by many manufacturers and researchers. Accurate prediction of the mechanical properties of hot-rolled aluminium alloys has become one of the hot topics in the development and application of aluminium alloys [1, 2]. Up to now, there are two main models in the field of metal property prediction. One of them is the construction of material constitutive models for material property prediction [3]. Jia et al. [4] used experimentally obtained stress-strain data to calculate the material constants involved in the Arrhenius-type constitutive model and the modified Zerilli–Armstrong (MZA) model. Zhang et al. [5] established the constitutive model for the thermal deformation behavior of high-strength aluminium alloy (Al-Zn-Mg-Cu). The results show that the constitutive model can accurately predict the flow behavior of the Al-Zn-Mg-Cu alloy. Although the emergence of the constitutive model enables researchers to reasonably predict the product performance according to the processing technology, the construction of the constitutive model still needs experimental support and reasonable assumptions, which leads to the fact that the constitutive model cannot fully meet the requirements of industrialization. To meet the needs of industrial production, another model emerged along with the maturity of computer technology, which uses intelligent algorithms to analyze large amounts of real production data to obtain more desirable predictions of mechanical properties. Along with the development of computer technology, artificial

intelligence algorithms play an increasingly important role in materials' research. Various machine learning algorithms applied to materials' research have solved many challenging problems [6]. The combination of computer technology and materials' science will likely yield more important achievements in the foreseeable future [7]. Guo et al. [8] proposed a method for multiproperty prediction of materials using the Interior Point Algorithm. The rationality and reliability of the above theory are verified successfully by the experiment using the data of the steel production process. Among the many machine learning algorithms on which statistical models rely, neural network-like algorithms are favored and widely used in the field of material property prediction due to their excellent properties [9, 10]. Niklas et al. [11] needed to develop accurate models to ensure efficient control equipment for superelastic shape memory alloys (SMA). After training, the ANN can successfully calculate model parameters from cyclic tensile stress-strain tests, thereby improving the efficiency of SMA control devices. Lan et al. [12] experimentally established a dataset of the chemical composition, processing parameters, and mechanical properties of the A380 alloy. The Fe/Mn content ratio, Sr content, cooling rate, and porosity content were the input variables, and ultimate tensile strength (UTS) and elongation (El) were used as output parameters. Two ANN models were developed, namely, (1) a back propagation artificial neural network (BP-ANN) model and (2) a back propagation artificial neural network model for particle swarm optimization (PSO-BP-ANN). The results show that the established PSO-BP-ANN model has better reliability and prediction accuracy than the BP-ANN model. Wu et al. [13] established an ANN model to predict the bending deformation in welded thin-walled aluminium alloy tube structures. The model's input variables include the four controllable position parameters of the weld, while the target output is the bending distortion in the x- and y-axis directions. A supervised multilayer feedforward back propagation (BP) neural network is proposed to estimate the bending distortion quickly and accurately. The predicted values of the designed BP neural network are compared with the finite element simulation results. The results show that the proposed BP neural network model can accurately predict the bending distortion caused by welding over a range of welding position parameters. Jaafreh et al. [14] used a multiobjective evolution (MOE) algorithm and machine learning techniques to predict the age-hardening behavior of aluminium alloy under various machining conditions. The results showed that combining the MOE algorithm and the machine learning process can successfully refine features and construct accurate machine learning prediction models compared to other feature selection and preprocessing methods. Sun et al. [15] used ANN methods to develop a correlation model between the thermal processing parameters and mechanical properties of Ti-6Al-4V alloy based on a series of forging and heat treatment experimental data. The correlation model was developed using the ANN method. The results show a reliable correlation between the process parameters and the mechanical properties of the Ti-6Al-4V alloy. Aykut et al. [16] improved the experimental model of surface roughness using ANN and response surface methodology (RSM).

ANN is widely used in various fields of material research [17, 18], but ANN is very time-consuming in the training process. To overcome this shortcoming, the ELM algorithm is proposed. ELM, an emerging single hidden layer neural network algorithm [19], has received attention in material property prediction research due to its fast learning speed and high generalization capability. Cao et al. [20] used ELM optimized by the genetic algorithm (GA) with other numerical models (including finite element model simulation) to determine the critical dimensions of prefabricated gear blanks with complex geometry for comparative analysis. The results showed that the GA-ELM and R-GPLVM predictions were in good agreement with the experimental results. Sui and Lv [21] combined the ELM algorithm-based model with an attribute reduction method. With the attribute reduction method combining information entropy and Gram–Schmidt orthogonal transformation, the process parameters that can effectively affect quality were selected to form a subset of features. Compared with traditional modelling methods, the model has the advantages of a simple structure, low time consumption, and high prediction accuracy. The prediction results show that the model has better adaptability to complex hot rolling processes, and the prediction performance is better than that of the traditional ELM model. Liu et al. [22] proposed a rolling force prediction method based on GA, PSO, and multihidden layer extreme learning machine (MELM), namely, the PSO-GA-MELM algorithm, which uses MELM as the primary model for rolling force prediction. In the modelling process, a genetic algorithm is used to determine the optimal number of hidden layers and nodes and a particle swarm algorithm is used to search for the optimal input weights and biases. Experimental results show that the rolling force prediction model trained by the algorithm has an excellent performance in prediction accuracy and can be used for the prediction of rolling force in the hot strip rolling process.

Although machine learning models, especially neural network type models, have been widely used in the study of steel materials, there has been little research in the prediction of mechanical properties of aluminium alloy materials. The main objective of this study is to develop an optimised ELM model that can accurately predict the mechanical properties of aluminium alloy strips. Firstly, the model is built using a dataset obtained from an aluminium alloy strip production line. Secondly, the ELM model was optimised using the GWO algorithm. Finally, a comparative analysis of the accuracy of the model was carried out. The experimental results show that the model is feasible to be applied to the prediction of mechanical properties of aluminium alloy strips.

2. A Brief Introduction to MGWO, GWO, and ELM

2.1. ELM Algorithm. ELM was born in 2004 to overcome the limitation of the complex and slow iterative structure of traditional neural networks. ELM's single hidden layer

feedforward neural network randomly selects the weights and biases of the number of hidden nodes. ELM has received a lot of attention from scholars since its introduction because, compared with traditional neural networks, ELM as single hidden layer feedforward neural networks (SLFNs) can have faster iteration speed and better generalization while ensuring accuracy [16]. The algorithm principle of ELM algorithm is shown in equations (1)–(7) [19]. The structure of the ELM algorithm is illustrated in Figure 1.

As illustrated in Figure 1, we suppose that there exist N samples $(\mathrm{X_i},\ \mathrm{t_i})$, where $\mathrm{X_i} = [\mathrm{x_{i1}}, \mathrm{x_{i2}}, \mathrm{x_{i3}}, \ldots, \mathrm{x_{in}},]^{\mathrm{T}} \in \mathrm{R^n}$, $\mathrm{t_i} = [\mathrm{t_{i1}}, \mathrm{t_{i2}}, \mathrm{t_{i3}}, \ldots, \mathrm{t_{im}},]^{\mathrm{T}} \in \mathrm{R^m}$, when the neural network has a hidden layer while that hidden layer has L hidden layer neurons, the output value of the neural network can be expressed as follows:

$$f_L\left(X_j\right) = \sum_{i=1}^{L} \beta_i g\left(W_i \bullet X_j + b_i\right), j = 1, 2, 3, \cdots, N, \quad (1)$$

where β_{i} is the output weight between the first i output weight between the neuron in the hidden layer and the neuron in the output layer, $g(\bullet)$ is the activation function, and $g(W_i \bullet X_j + b_i)$ represents the input parameter X_j of the output of the first i output of the hidden layer neuron. $W_i = [w_{i1}, w_{i2}, w_{i3,} \ldots, w_{in}]^T$ is the input weight between the first i input weight between the first input neuron and the hidden layer neuron, and b_i is the output bias of the first i output bias of the first hidden layer neuron, and $W_i \bullet X_j$ denotes W_i as the inner product of X_j of the inner product.

The smaller the error between the predicted and measured values of a single hidden layer neural network, the more accurate the model's prediction results, as shown in the following equation:

$$\sum_{j=1}^{N} \left\| f_L\left(X_j\right) - t_j \right\| = 0, \quad (2)$$

i.e., parameters $\beta_i W_i$ and b_i exist as shown in the following equation:

$$f_L\left(X_j\right) = \sum_{i=1}^{L} \beta_i g\left(W_i \bullet X_j + b_i\right) = t_j, j = 1, 2, 3, \cdots, N. \quad (3)$$

In the matrix form, this can be expressed as shown in the following equation:

$$H\beta = T, \quad (4)$$

of which $\mathrm{H}(W_1, W_2, \cdots, W_L, b_1, b_2, \cdots, b_L, X_1, X_2, \cdots, X_L) = \begin{bmatrix} g(W_1 \bullet X_1 + b_1) & \cdots & g(W_L \bullet X_1 + b_L) \\ \vdots & \ddots & \vdots \\ g(W_1 \bullet X_N + b_1) & \cdots & g(W_L \bullet X_N + b_L) \end{bmatrix}_{N \times L}$, $\beta = \begin{bmatrix} \beta_1^T \\ \vdots \\ \beta_L^T \end{bmatrix}_{L \times m}$, $T = \begin{bmatrix} T_1^T \\ \vdots \\ T_L^T \end{bmatrix}_{N \times m}$, H represents the output of the nodes in the hidden layer, and β represents the output weights from the hidden layer to the output layer. T represents the desired output value with high prediction accuracy. As shown in equation (5), to obtain a single hidden layer neural network with the desired prediction accuracy, the parameters β^*, W^*, and b^* are desired to be obtained.

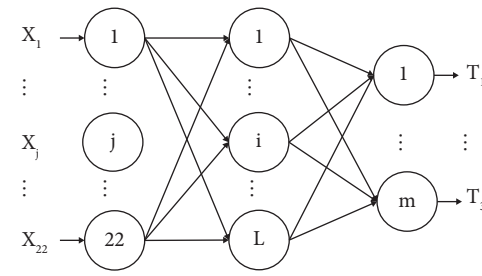

Figure 1: Network structure of the ELM algorithm.

$$\left\| H(W^*, b^*, X_i)\beta^* - T \right\| = \min_{W,b,\beta} \left\| H(W_i, b_i, X_i)\beta_i - T \right\|, \quad (5)$$

where $i = 1, 2, 3, \cdots, L$, is equivalent to making the loss function J obtain its minimum value, as shown in the following equation:

$$J = \min_{W,b,\beta} \sum_{j=1}^{N} \left(\sum_{i=1}^{L} \beta_i \mathrm{g}\left(\mathrm{W}_i \bullet \mathrm{X_j} + \mathrm{b}_i\right) - \mathrm{t_j} \right)^2. \quad (6)$$

The process of training a single hidden layer neural network can be transformed into solving $H\beta = T$, which can solve for the matrix H of the Moore–Penrose generalized inverse matrix $H^{\dagger}$. Due to the characteristics of the ELM itself, i.e., the input weights W_i and the hidden layer bias $\mathrm{b_i}$ are determined randomly. Once the input weights W_i and hidden layer bias $\mathrm{b_i}$ are determined, the output matrix of the hidden layer H is uniquely determined. At this point, $H^{\dagger}$ is the matrix H of the Moore–Penrose generalized inverse, as shown in the following equation:

$$\beta^* = H^{\dagger}\mathrm{T}. \quad (7)$$

2.2. GWO Algorithm. The GWO algorithm is inspired by the hunting behavior of the grey wolf pack and is designed to simulate the group collaboration behavior of the grey wolf pack in the process of predation to achieve the purpose of optimization [23]. The GWO algorithm has an adaptive convergence factor and a feedback mechanism that allows it to avoid falling into the trap of local optimality in the global search process. It, therefore, has higher accuracy and robustness in the problem-solving process.

The grey wolf is a canine predator that prefers to live in packs, with a clear hierarchical division of labor among its members during the hunt. The hierarchical distribution of the grey wolf population is similar to the pyramid's structure, as shown in Figure 2. The pack's leader is located at the first level of the pyramid and is called α. The think tank team of the pack at the second level of the pyramid is called β. β is second only to α in terms of leadership in the pack, and when there is a vacancy in α's position in the pack, β will fill the vacant position and become the new α. The executors of the pack are located at the third level of the pyramid and are

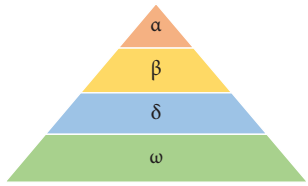

Figure 2: Hierarchy chart of the grey wolf population.

called δ. The wolves at the bottom of the pyramid are called ω and are responsible for executing $\alpha\beta$ and δ's commands. The strict hierarchical distribution is directly reflected in the hunting activities of the grey wolf, which will be led by α. During the hunting process, $\alpha\beta\delta$ and ω will strictly follow their duties and have a clear division of labor and the hunting process can be divided into three main steps, namely, finding and surrounding the prey; harassing and tracking the prey; and attacking the prey.

The algorithm principle of the GWO algorithm is shown in equations (8)–(15) [23]. The grey wolf optimization algorithm abstracts the hunting pattern of a wolf pack into an optimization algorithm. In the process of finding and encircling prey, the grey wolf's process of encircling prey is defined in equations (8) and (9) as follows. Equation (8) represents the distance between the grey wolf and the prey. Here, $\vec{D}$ represents the direction and distance travelled by individual grey wolves. $\vec{C}$ is the parameter used to determine the direction of the wolf pack's search for prey, t represents the number of iterations of grey wolf positions, and $\vec{X}_P(t)$ represents the position that individual grey wolves tend to approach. $\vec{X}(t)$ represents the position of the individual grey wolf when the iteration number is t. Equation (9) represents the iterative formula for the position of the grey wolf, and $\vec{A}$ is the parameter used to adjust the radius of the prey search. $\vec{A}$ and $\vec{C}$ calculation formulas are shown in equations (10) and (11). a is the convergence factor, as shown in equation (12), and a decreases from a maximum value of 2 until it becomes 0 as the number of iterations increases. $\vec{r_1}$ with $\vec{r_2}$ is a random vector with the modulus length set in the range [0, 1].

$$\vec{D} = \left|\vec{C} \bullet \vec{X}_P(t) - \vec{X}(t)\right|, \tag{8}$$

$$\vec{X}(t+1) = \vec{X}_P(t) - \vec{A} \bullet \vec{D}, \tag{9}$$

$$\vec{A} = 2a \bullet \vec{r_1} - a, \tag{10}$$

$$\vec{C} = 2\vec{r_2}, \tag{11}$$

$$a = 2 - \frac{2t}{t_{\max}}. \tag{12}$$

In the practical application of the optimization algorithm, the optimal three solutions are assigned to α, β, and δ according to their fitness, making $\alpha\beta\delta$ the leader of the pack closest to the prey. In turn, the other grey wolves adjust their positions according to the best-positioned grey wolf, calculate their fitness after the position update, and rerank the grey wolves according to their fitness size. The mechanism for individuals in the pack to update their positions is shown in Figure 3. The mathematical model of individual grey wolves updating their positions can be shown as equation (13). Here, $\vec{D}_\alpha\ \vec{D}_\beta\ \vec{D}_\delta$ represents the distance relationship between α and β δ individuals and other individuals, respectively, $\vec{X}_\alpha\ \vec{X}_\beta\ \vec{X}_\delta$ represents, respectively, the $\alpha\beta\delta$ the current position of the individual, $\vec{C}_1\ \vec{C}_2\ \vec{C}_3$ represents a random vector, and $\vec{X}$ represents the current position of an individual grey wolf. In a wolf pack ω, the distance and direction of the individual to the target are shown in equations (14) and (15).

$$\begin{cases} \vec{D}_\alpha = \left|\vec{C}_1 \bullet \vec{X}_\alpha - \vec{X}\right|, \\ \vec{D}_\beta = \left|\vec{C}_2 \bullet \vec{X}_\beta - \vec{X}\right|, \\ \vec{D}_\delta = \left|\vec{C}_3 \bullet \vec{X}_\delta - \vec{X}\right|, \end{cases} \tag{13}$$

$$\begin{cases} \vec{X}_1 = \left|\vec{X}_\alpha - A_1 \bullet \vec{D}_\alpha\right|, \\ \vec{X}_2 = \left|\vec{X}_\beta - A_2 \bullet \vec{D}_\beta\right|, \\ \vec{X}_3 = \left|\vec{X}_\delta - A_3 \bullet \vec{D}_\delta\right|, \end{cases} \tag{14}$$

$$\vec{X}(t+1) = \frac{\vec{X}_1 + \vec{X}_2 + \vec{X}_3}{3}. \tag{15}$$

From equations (10) and (12), the value of a will gradually decrease with the progress of iteration and the fluctuation range of parameter $\vec{A}$ will also decrease. The grey wolf algorithm uses the $|\vec{A}|$ and $\vec{C}$ to avoid the solution of the optimization algorithm falling into a local optimum. As shown in Figure 4(a), when $|\vec{A}| > 1$, the grey wolf individual moves away from the target, i.e., a global search is performed. As shown in Figure 4(b), when $|\vec{A}| < 1$, the individual grey wolf will launch a final attack on the prey, i.e., the optimal solution is obtained. From equation (11), it can be seen that C is a random value taking values in the interval [0, 2]. C represents the size of the hindrance for the grey wolf to approach the prey. $C > 1$ means that the grey wolf individual is not easy to approach the target; on the contrary, $C < 1$ means that the grey wolf individual is easy to approach the target and C can maintain randomness during the iterative process and helps the algorithm escape in time when it is about to fall into a local optimum trap. This algorithm feature also contributes to the ease with which the grey wolf optimization algorithm can obtain a global optimum.

2.3. MGWO Algorithm. The MGWO algorithm was proposed by Zhang and Zhou [24] in 2021. The algorithm considers that a with different update strategies can significantly affect the algorithm's performance [25]. The algorithm principle of the MGWO algorithm is shown in equations (16)–(18) [24]. It uses a convergence factor update based on regular exponential changes, as shown in equation (16). In addition, to enhance the balance between global search and local exploitation, the MGWO algorithm proposes a new adaptive shifting strategy [24, 26], whose

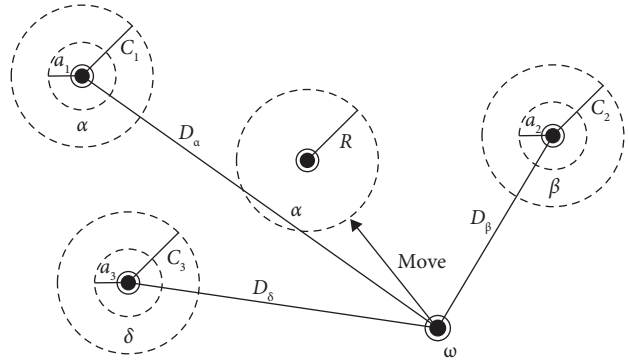

Figure 3: Schematic of the grey wolf location update for the grey wolf algorithm.

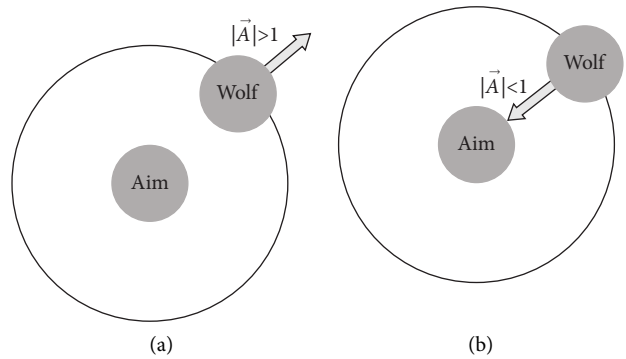

Figure 4: Individual grey wolves (a) moving away from their target and (b) attacking their prey.

mathematical expression is shown in equation (17). Here, the weights W_i of the mathematical expression are shown in equation (18).

$$a = 2e^{(-t/)}t_{\max}, \tag{16}$$

$$\vec{X}(t+1) = \frac{W_1\vec{X}_1 + W_2\vec{X}_2 + W_3\vec{X}_3}{3}\left(1 - \frac{t}{t_{\max}}\right) + \vec{X}_1\frac{t}{t_{\max}}, \tag{17}$$

$$W_i = \frac{\left|\overrightarrow{X_i}\right|}{\left|\overrightarrow{X_1}\right| + \left|\overrightarrow{X_2}\right| + \left|\overrightarrow{X_3}\right|}, \mathrm{i} = 1, 2, 3. \tag{18}$$

3. Proposed GWO-ELM Prediction Model

ELM is an effective mechanism for pattern classification and regression learning. In the ELM algorithm model, the number of hidden layer neurons needs to be determined in advance and the structure of the neural network has a direct impact on the accuracy of the ELM algorithm model, which relies on a large number of hidden layer nodes for good performance. As the number of nodes in the hidden layer increases, the computational cost increases significantly [27]. An excessive number of hidden layer neurons will make an ELM model so complex that it will slow down the prediction speed or even overfit. However, too few hidden layer neurons will result in an ELM model that does not achieve the desired accuracy. To date, there is no accepted and valid theory to guide the selection of the number of hidden layer neurons. In most cases, the determination of the number of hidden layer neurons relies on the experience of the model trainer to obtain the appropriate neural network parameters. If the essential parameters of the algorithm depend too much on manual selection, then the robustness of the model will be reduced. In addition, the weights and biases of the ELM model are randomly generated, which simplifies the algorithm but also has a significant negative impact on the algorithm's accuracy, as the randomness of the parameters makes the model's accuracy highly uncertain.

Mean Absolute Percentage Error (MAPE) mean square error (MSE) and root mean square error (RMSE) will be used to evaluate the performance of the model. The calculation methods of MAPE MSE RMSE and R^2 are shown in equations (19)–(22), respectively [15].

$$MAPE = \frac{100\%}{n}\sum_{i=1}^{n}\left|\frac{\dot{\hat{y}}_i - y_i}{y_i}\right|, \tag{19}$$

$$MSE = \frac{1}{n}\sum_{i=1}^{n}\left(\dot{\hat{y}}_i - y_i\right)^2, \tag{20}$$

$$RMSE = \sqrt{\frac{1}{n}\sum_{i=1}^{n}\left(\dot{\hat{y}}_i - y_i\right)^2}, \tag{21}$$

$$R^2 = \frac{SSR}{SST} = \frac{\sum_{i=1}^{n}\left(\dot{\hat{y}}_i - \overline{y}\right)^2}{\sum_{i=1}^{n}\left(y_i - \overline{y}\right)^2}, \tag{22}$$

where n represents the number of samples to be substituted into the formula for operation, $\dot{\hat{y}}_i$ represents the predicted value, y_i represents the actual value, and $\overline{y}$ represents the mean.

The suitable combination of the number of hidden layer neurons with the input weights and biases becomes the focus of improving the prediction accuracy of ELM. Therefore, this paper introduces the GWO algorithm to optimize the ELM algorithm, forming a new hybrid algorithm named GWO-ELM. The flow of the GWO-ELM algorithm is shown in Figure 5. In the modelling process of the GWO-ELM algorithm, the population size, objective function, and the maximum number of iterations of the GWO algorithm are first determined. Then, the optimal number of hidden layer neurons, the optimal input weights, and optimal bias of the ELM network are determined using the GWO algorithm. The GWO algorithm then determines the optimal number of hidden layer neurons, the optimal input weights, and the ELM network's optimal bias.

The specific steps of the GWO-ELM algorithm are as follows:

(1) We determine the input data. The raw data were preprocessed and randomly divided into training and test sets.

(2) We initialize the GWO algorithm and determine the number of grey wolves in the grey wolf algorithm population, the maximum number of iterations, and the number of parameters to be optimized. We determine the parameters A and C. We take $i = 0$.

(3) We initialize the weights and biases of the ELM, at which point the number of hidden layer neurons is no longer determined empirically but by experimental comparison. At this point, the number of hidden layer neurons is $L = i + 1$.

(4) We calculate the fitness of each individual in the pack to determine the best individual, in which MAPE is used as the individual's fitness. The smaller the error of an individual, the better it is. We determine α, β, δ, and ω in the wolf pack based on the individual error in the pack.

(5) We update the position and parameters of each grey wolf a A and C.

(6) We update the input weight ω and the bias b of the ELM model from the results of step (5) so that the parameters of the ELM model take values closer to the optimal values.

(7) We calculate the fitness of all grey wolves and update $\alpha\beta\delta$ and its fitness. The individual prediction error size determines that individual's leadership position in the wolf pack. That is, the $\alpha\beta\delta$ of wolves is determined according to the error of individual prediction values from small to large.

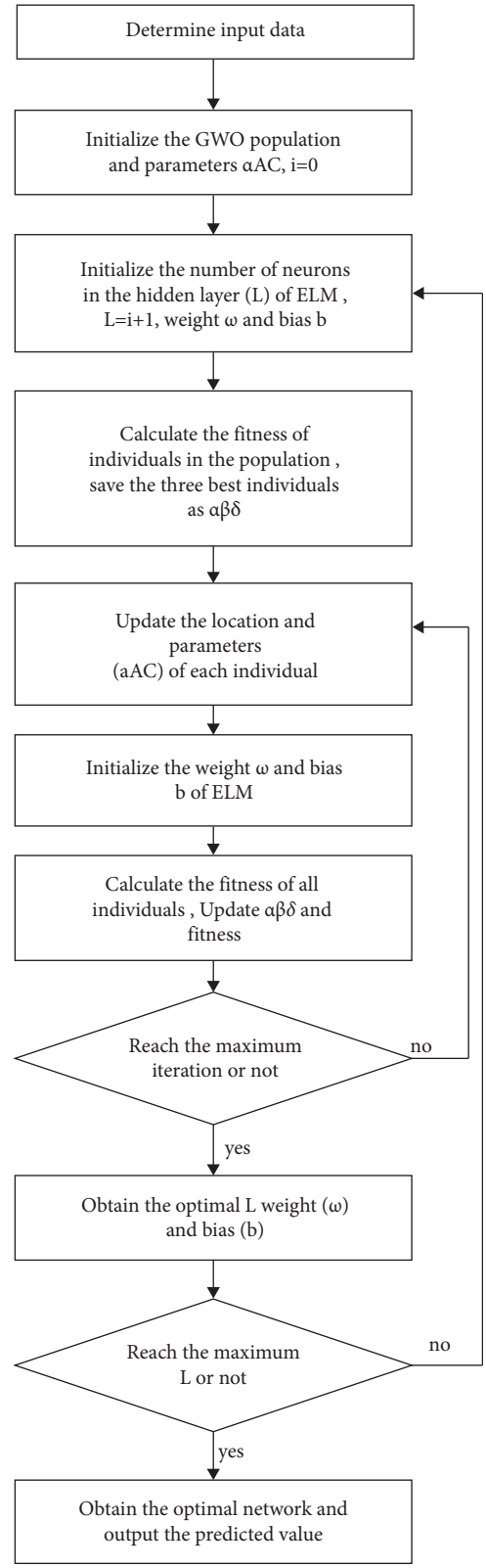

Figure 5: Flow chart of the GWO-ELM algorithm.

(8) We determine whether the maximum number of iterations is reached; if not, we return to step (5); otherwise, the optimal limit learning machine

structure is obtained when the number of neurons in the hidden layer is L.

(9) To determine whether L reaches the maximum number of hidden layer neurons. If it does not reach the maximum number of hidden layer neurons, step (3) is repeated; otherwise, the model's prediction accuracy can be compared when L takes different values. Finally, the optimal ELM network structure can be obtained.

4. Model Structure Building and Experimental Analysis

Extensive experiments were conducted to test the prediction accuracy of the proposed GWO-ELM model and compare and analyze the performance of the GWO-ELM model with that of the conventional ELM model and the MGWO-ELM model.

4.1. Acquisition and Processing of Training Samples. The prediction performance of the extreme learning machine is very dependent on the quality of the input data, and redundant or conflicting data will not result in the desired prediction accuracy [28]. High-quality data are the basis for establishing accurate models. This paper uses the actual production data of Shandong Nanshan Aluminum Industry Co., LTD, as experimental data. The data come from the big data platform database of the enterprise. This data are available and can be obtained as shown in the Data Availability section. The test standard number GB/T 16865-2013 was used to obtain data on material properties. In the experiments of this paper, the correlation between the input and output parameters was first analyzed using correlation analysis algorithms and physical metallurgy principles. Parameters with significant influence on tensile strength, yield strength, and elongation were selected as input parameters for the model, and a total of 22 input parameters were extracted. The input parameters of the model are shown in Table 1. This data are available and can be obtained as shown in the Data Availability section. The output parameters were set to tensile strength, yield strength, and elongation, and the output parameters are shown in Table 2. Table 1 shows the statistics for the mean, standard deviation, and minimum and maximum values for each input parameter. Table 2 shows each output parameter's mean, standard deviation, and minimum and maximum value statistics. After removing the outlier data for the initially identified parameters, the mean values were used to fill in the vacant values. The processed data will be used for model training and testing. A total of 131 production data sets on 6-series aluminium alloys and 5-series aluminium alloys were collected and applied. The main compositions of the aluminium alloys used for the data in this paper are shown in Table 3. Seventy percent of the total data (91 sets) will be assigned to the training set and used to train the model to have the desired prediction accuracy. The remaining data (40 sets) will be allocated to the test set to test the model's performance.

Data processing needs to avoid the adverse impact of the difference in the order of magnitude between different parameters on the prediction results, so the input parameters need to be normalized before input into the model. The input parameters need to be normalized before being fed into the model. The data normalization method is shown in equation (23), the input parameters will be normalized to [0, 1] [29]. Here, x represents the normalized data, $x_{\max}$ and $x_{\min}$ represent the maximum and minimum values of data in the dimension, respectively, and x_i represents the normalized result.

$$x_i = \frac{x - x_{\min}}{x_{\max} - x_{\min}}. \tag{23}$$

4.2. Determination of the Parameters of the GWO-ELM Algorithm. The network structure of the GWO-ELM model is closely related to the data structure. The dimensionality of the input determines the number of neurons in the input layer. The dimensionality of the output determines the number of neurons in the output layer. The input parameter is 22 dimensions, so the number of neurons in the input layer is set to 22; the output parameter is 3 dimensions, so the number of neurons in the output layer is set to 3. In the following experiment, 70% of the data will be used to train the model and the remaining 30% will be used to test the performance of the model. The entire simulation process in this experiment was carried out using Python 3.6. Firstly, the activation function was determined by the experiment [30]. The number of neurons in the hidden layer was tentatively set to 22 to test the model's prediction accuracy with different activation functions. The experimental results are shown in Table 4. The mean square error of the test set and the mean absolute percentage error of the test set were minimized when the activation function was "sigmoid." The mean squared error of the training set for the "sigmoid" activation function is 316.72, the mean squared error of the test set is 594.99, and the total mean squared error of the prediction is 401.68. The mean squared error of the training set for the "sigmoid" activation function and the mean absolute percentage error for the training set are 8.02, the mean absolute percentage error for the test set is 10.45, and the total mean absolute percentage error is 8.76. The ELM algorithm activation function is set to "sigmoid."

Next, experiments are used to determine the optimal number of hidden layer neurons for the ELM algorithm. The number of hidden layer neurons has a large impact on the prediction results of the ELM model, and too many or too few hidden layer neurons will decrease the model's prediction accuracy. In this section, the ELM activation function is "sigmoid" and the other parameters remain unchanged. The number of ELM hidden layer neurons was determined to be in the range [1, 38] based on the dimensionality of the input parameters used in this experiment. The performance of the ELM model with different numbers of hidden layer neurons was compared, and the results are shown in Figure 6. When the number of neurons in the hidden layer was less than 23, for tensile strength, yield

Table 1: Statistical information on input parameters.

Number	Parameter	Unit	Mean	Std	Min	Max
1	Machine speed	(m/min)	21.352	8.735	7.0	48.0
2	Heating temperature-1	(°C)	418.130	100.595	314.9	575.0
3	Heating temperature-2	(°C)	419.368	101.832	314.8	575.1
4	Heating temperature-3	(°C)	419.094	101.684	314.8	575.0
5	Heating temperature-4	(°C)	418.385	101.255	315.1	575.0
6	Heating temperature-5	(°C)	418.247	101.283	314.9	574.9
7	Heating temperature-6	(°C)	417.496	100.936	315.0	575.2
8	Heating temperature-7	(°C)	417.301	101.120	310.4	575.3
9	Heating temperature-8	(°C)	417.449	101.091	310.4	575.7
10	Heating temperature-9	(°C)	417.466	101.057	310.5	575.5
11	Heating temperature-10	(°C)	417.507	101.047	310.5	575.6
12	Heating temperature-11	(°C)	417.398	101.079	310.6	575.4
13	Heating temperature-12	(°C)	412.836	104.010	309.8	574.9
14	Elongation of tension bending straightening 1	(%)	0.312	0.454	0	1.0
15	Preageing temperature 1	(°C)	19.535	4.991	11.0	33.3
16	Preageing temperature 2	(°C)	19.973	5.46918	11.2	38.1
17	Preageing speed	(m/min)	22.267	8.290	8.0	49.0
18	Coiling tension	(N/mm^2)	12.008	0.488	7.0	13.0
19	Depression distance of tension bending straightening	(mm)	0.428	0.273	0.036	0.979
20	Pretension of tension bending straightening	(N/mm^2)	50.088	15.883	17.0	90.0
21	Post-tension of tension bending straightening	(N/mm^2)	50.088	15.883	17.0	90.0
22	Elongation of tension bending straightening 2	(%)	0.312	0.454	0	1.0

Table 2: Statistical information on output parameters.

Number	Parameter	Unit	Mean	Std	Min	Max
1	Tensile strength	MPa	263.789	43.507	204.000	338.667
2	Yield strength	MPa	212.830	61.052	93.667	309.500
3	Elongation	%	14.366	3.460	7.500	26.667

Table 3: Main components of aluminium alloy strip.

	Element	Al (%)	Mg (%)	Si (%)	Fe (%)	Cu (%)	Cr (%)	Mn (%)	Ti (%)	Ga (%)	Others (%)
Mass	6xxx	97.12	1.0122	0.6931	0.5564	0.2391	0.2301	0.084	0.025	0.0166	0.028
percentage	5xxx	94.37	4.7273	0.0969	0.2498	0.0674	0.0335	0.3961	0.0191	0.0141	0.022

Table 4: Comparison of different activation functions.

Name	MSE			MAPE		
	Train set	Test set	All	Train set	Test set	All
Sigmoid	316.72	594.99	401.68	8.02	10.45	8.76
tanh	498.75	1052.36	667.79	10.25	14.29	11.49
Linear	196.76	2544.63	913.65	7.55	13.10	9.25
rbf_l1	18150.11	22051.90	19341.50	49.48	52.97	50.54
rbf_l2	405.53	901.78	557.06	9.38	11.79	10.12

strength, and elongation, the prediction accuracy of the test set increased with the increase of the number of neurons. When the number of neurons in the hidden layer exceeds 23, especially the prediction accuracy of elongation, the prediction accuracy of the test set shows a trend of fluctuation decline. The reason for the previously mentioned phenomenon is that with the increase of the number of hidden layer neurons, the overfitting tendency of the model increases and the overfitting leads to the abnormal increase of the prediction error of the test set. As shown in Figure 6, the prediction accuracy reached its peak when the number of hidden layer neurons was 23.

Next, the population size of the grey wolf algorithm was determined by experiments. The number of iterations was set to 300, and the number of individuals in the population ranged from [10, 100]. The prediction results of the test set

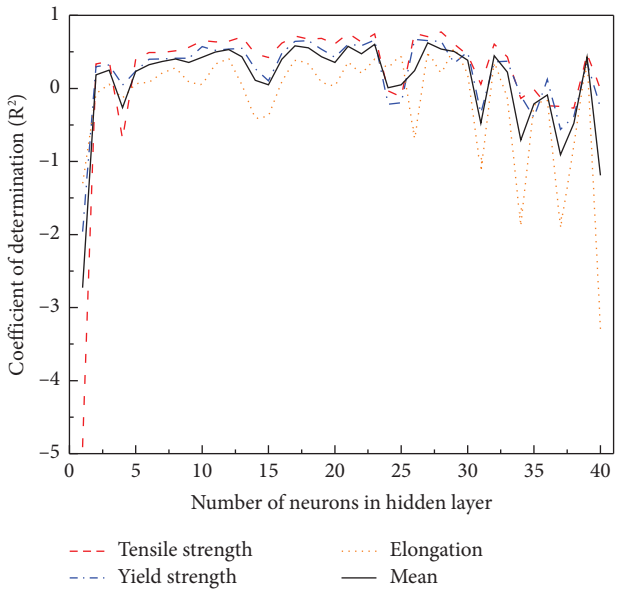

Figure 6: The prediction accuracy of the test set with the number of hidden layer neurons.

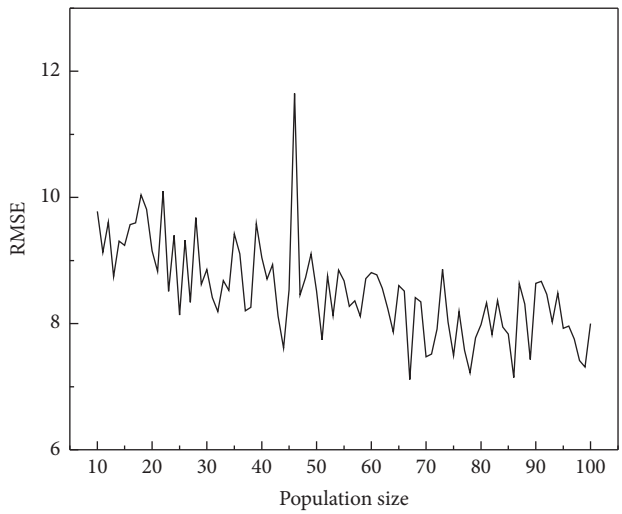

Figure 7: Population size and test set error trends.

with the number of iterations are shown in Figure 7. The prediction results of the test set showed low prediction errors when the population size was 67, 78, and 86. Still, too large population would cause the model training time to be extended, resulting in unnecessary time wastage.

The choice of objective function has a massive impact on the performance of the GWO algorithm. When the model is a multioutput algorithm, the influence of the weights between different objectives on the prediction accuracy of the final algorithm is of interest. To investigate the effect of the objective function weights on the mechanical properties of aluminium alloys, the objective function used in this paper is shown in equation (24). Here, P_T, P_Y, and P_E are the predicted values of tensile strength, yield strength, and elongation, respectively; E_T E_Y E_E are the measured values of tensile strength, yield strength, and elongation, respectively; N is the number of measured values; ji is the penalty coefficient of yield strength and elongation, respectively. The number of iterations of the GWO algorithm is set to 100, and the trends of tensile strength, yield strength, and elongation with the change of penalty coefficients are shown in Figure 8. As an example, Figure 8(a) shows the relationship between the MAPE error of tensile strength and the penalty coefficient. The closer the color was to dark, the smaller the MAPE error and the better the prediction accuracy. Different combinations of the penalty coefficient correspond to different prediction accuracies of mechanical properties. When the combination of penalty coefficients (i, j) is (20, 80), (90, 50), (60, 30), and (90, 80), the prediction error of tensile strength is small. Similarly, after comparing Figures 8(b) and 8(c), the penalty coefficient corresponding to the minimum prediction error of yield strength and elongation can be obtained. The prediction errors of yield strength and elongation of tensile strength are summarized. When the penalty coefficient (i, j) is (20, 80), the prediction errors of three mechanical properties are smaller at the same time.

The trend of variance of MAPE for the three output variables is shown in Figure 9, which indicates that when the penalty coefficients ji are 80 and 20, respectively, the corresponding MAPE variances for tensile strength, yield strength, and elongation are smaller. When the penalty coefficients are 80 and 20, respectively, the predicted values of tensile strength, yield strength, and elongation can maintain a balance of the predicted values of the three mechanical properties while ensuring a small accuracy of their own. The penalty coefficients in the objective function equation (23) ji are chosen as 80, 20. The comparison between the optimal penalty coefficient and the original coefficient is shown in Table 5. The optimal penalty coefficient can not only reduce the MAPE of the test set but also significantly reduce the variance of the prediction errors of the three variables. A lower variance means that the prediction error distribution of the three variables is more balanced.

$$P\left(P_T, P_Y, P_E\right) = \frac{1}{n}\left(\sum_{i=1}^{n}\left|\frac{P_T - E_T}{E_T}\right| + j \times \sum_{i=1}^{n}\left|\frac{P_Y - E_Y}{E_Y}\right| + i \times \sum_{i=1}^{n}\left|\frac{P_E - E_E}{E_E}\right|\right) \times 100\%, i, j = 1, 10, 20 \cdots 100. \quad (24)$$

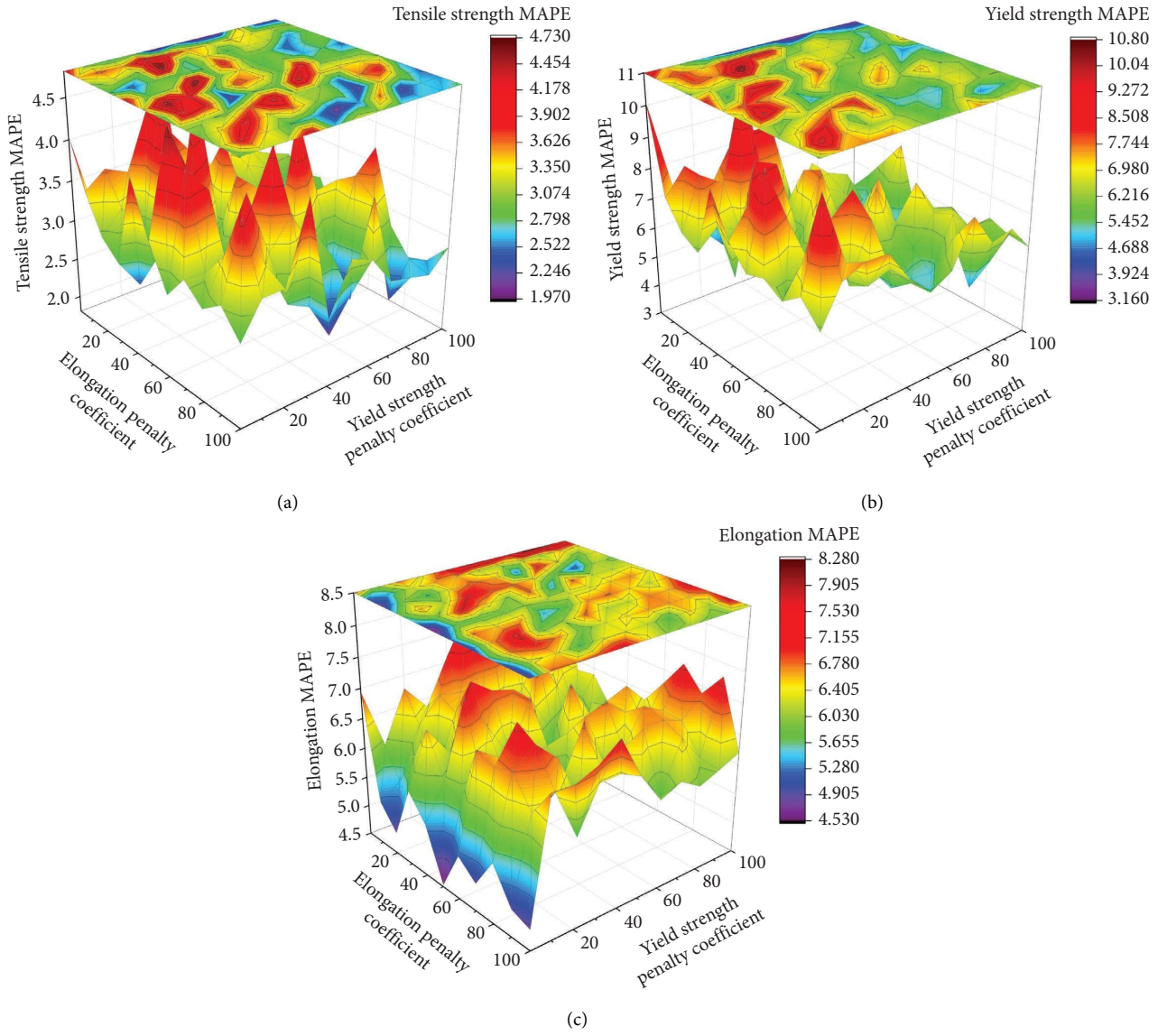

Figure 8: Trend of the test set MAPE with the penalty factors: (a) tensile strength, (b) yield strength, (c) and elongation.

The number of iterations of the GWO algorithm significantly impacts the prediction results, and each iteration will obtain a better value of the ELM algorithm parameters than the previous iteration. The GWO algorithm population size was set to 30, the fitness function was set to equation (24), and $i = 20$, $j = 80$. The relationship between the prediction accuracy of the GWO-ELM model test set and the number of iterations, as well as the model training time and the number of iterations, is shown in Figure 10. As the iterations proceeded, the R^2 of the test set increases gradually and the modelling time increased linearly with the number of iterations. When the number of iterations reaches 3150, the prediction accuracy of tensile strength, yield strength, and elongation converges.

In summary, the parameters of the GWO-ELM algorithm have been determined and are shown in Table 6. When the values of parameters are shown in Table 6, the iterative optimization of weight ω and bias b by the GWO algorithm can be realized. Thus, when the maximum number of iterations is reached, the optimal input weight ω and bias b of the ELM network in the GWO-ELM model are determined.

4.3. Experimentation and Evaluation of Model Performance. In this section, mechanical property prediction experiments demonstrate the excellent prediction accuracy of the proposed GWO-ELM model. The model comparison experiment of the GWO-ELM model, MGWO-ELM model, and traditional ELM model is designed to verify the advantages of the proposed GWO-ELM model. Each model was run through twenty replicates, and the results were averaged to avoid misleading results from model chance.

To ensure a fair comparison, the corresponding parameters for the GWO-ELM model and the ELM model in this experiment are shown in Table 6. The parameters used by the MGWO algorithm are consistent with the GWO

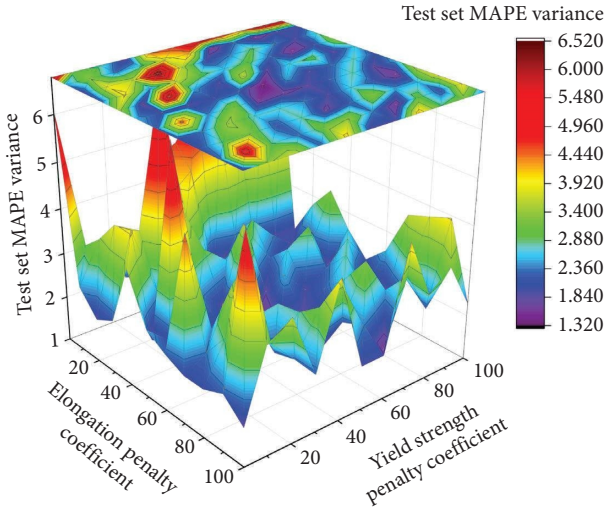

Figure 9: Trend of MAPE variance with the penalty coefficient for the test set of the three output variables.

Table 5: Optimal penalty factor vs. original factor.

i	j	Test set MAPE (%)			Train set MAPE (%)			Variance	
		Tensile strength	Yield strength	Elongation	Tensile strength	Yield strength	Elongation	Test set	Train set
1	1	4.04811	10.09929	6.94424	2.57422	6.30288	8.76849	6.107	6.483
20	80	3.17806	6.50873	6.41047	2.80229	6.35357	7.42699	2.395	3.906

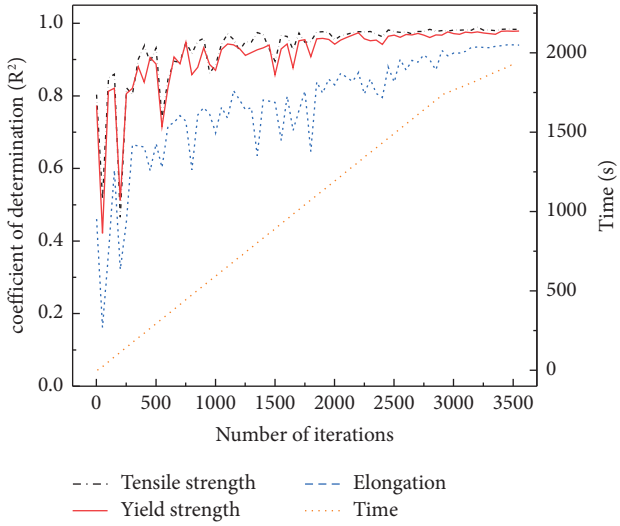

Figure 10: Prediction error and modeling time for the test set.

algorithm. MAPE and RMSE were error measures for the mechanical properties' prediction models. The prediction errors of the three models after twenty replicate experiments for the three mechanical properties are shown in Table 7. Table 7 provides an excellent visual representation of the prediction results of the GWO-ELM model, MGWO-ELM model, and ELM model for the three mechanical properties. In the test set, RMSE errors of tensile strength of the GWO-ELM model, MGWO-ELM model, and ELM model are 5.365, 11.557, and 21.489, respectively. The RMSE errors of yield strength in the GWO-ELM model, MGWO-ELM model, and ELM model are 11.881, 20.465, and 43.313, respectively. The RMSE errors of the elongation in the GWO-ELM model, MGWO-ELM model, and ELM model are 1.268, 1.848, and 5.360, respectively. The above-mentioned result indicates that the GWO-ELM model mentioned in this paper has a significantly higher prediction accuracy than the conventional ELM model for the three mechanical properties of tensile strength, yield strength, and elongation. The MGWO-ELM model outperforms the ELM

Table 6: Optimal parameter configuration for the GWO-ELM model.

Algorithm	Parameters	Configuration
GWO	Number of iterations	3150
	Population size	67
	Penalty coefficient [i, j]	[20, 80]
ELM	Number of neurons (input layer)	21
	Number of neurons (output layer)	3
	Number of neurons (hidden layer)	23
	Activation functions	Sigmoid

Table 7: Comparison of the predictive performance of the three models.

Mechanical properties	Name	RMSE		MAPE		R^2	
		Train set	Test set	Train set	Test set	Train set	Test set
Tensile strength	GWO-ELM	9.052	5.365	1.951	1.703	0.9549	0.9857
	MGWO-ELM	7.939	11.557	1.574	2.316	0.9534	0.9805
	ELM	10.976	21.489	2.702	5.317	0.9386	0.7102
Yield strength	GWO-ELM	15.499	11.881	4.204	2.703	0.9303	0.9662
	MGWO-ELM	16.795	20.465	4.225	5.185	0.9022	0.9804
	ELM	19.163	43.313	6.176	16.165	0.9053	0.3958
Elongation	GWO-ELM	1.424	1.268	7.371	5.994	0.7649	0.9141
	MGWO-ELM	1.355	1.845	6.937	9.244	0.8123	0.9074
	ELM	1.630	5.360	8.864	19.630	0.7384	−0.8312

model but is weaker than the GWO-ELM model. In the test set, for tensile strength, yield strength, and elongation, the MAPE of the GWO-ELM model is 1.703, 2.703, and 5.994 respectively, while the corresponding MAPE of the MGWO-ELM model is 2.316, 5.185, and 9.244 respectively, and that of the ELM model is 5.317, 16.165, and 19.630, respectively. The abovementioned result indicates that the average accuracy of the GWO-ELM model is significantly higher than that of the MGWO-ELM model for the three mechanical properties of tensile strength, yield strength, and elongation. R^2 was used as the evaluation index to evaluate the prediction results of the test set. The R^2 values of tensile strength in GWO-ELM, MGWO-ELM, and ELM models were 0.9857, 0.9805, and 0.7102, respectively. The R^2 values of yield strength in GWO-ELM, MGWO-ELM, and ELM models were 0.9662, 0.9804, and 0.3958, respectively. The R^2 values of elongation in GWO-ELM, MGWO-ELM, and ELM models were 0.9141, 0.9074, and −0.8312, respectively. The abovementioned results show that GWO-ELM and MGWO-ELM achieve an ideal fitting effect in the prediction of tensile strength, yield strength, and elongation, and the performance of the two models is far better than that of the ELM model. In addition, GWO-ELM was better than MGWO-ELM in the prediction of tensile strength and elongation, so the GWO-ELM model was slightly better than MGWO-ELM.

The predicted results of the GWO-ELM model, MGWO-ELM model, and ELM model compared to the actual values after twenty replicate experiments for the three mechanical properties are shown in Figure 11. Both in the training set and the test set, the prediction accuracy of the yield strength and elongation of the tensile strength is higher in the GWO-ELM model and the fit degree of the yield strength and elongation of the tensile strength is higher in the GWO-ELM model. The error distributions of the three model test sets are shown in Table 8. For the three mechanical properties of tensile strength, yield strength, and elongation, the GWO-ELM model has a more obvious advantage in the prediction results of the test set. This is especially true for the tensile and yield strengths. When the prediction deviation is controlled within ±10%, the prediction accuracy of tensile strength in the GWO-ELM model, MGWO-ELM model, and ELM model is 100%, 97.5%, and 80%, respectively. The prediction accuracy of yield strength of the GWO-ELM model, MGWO-ELM model, and ELM model is 97.5%, 92.5%, and 62.5%, respectively. The prediction accuracy of elongation in the GWO-ELM model, MGWO-ELM model, and ELM model is 77.5%, 77.5%, and 37.5%, respectively. Although the prediction accuracy of elongation of GWO-ELM and MGWO-ELM is the same when the error is controlled within ±10%, the prediction accuracy of the GWO-ELM model is better than that of MGWO-ELM when the prediction error is 5%. The abovementioned results indicate that the prediction accuracy of GWO-ELM is more stable than MGWO-ELM and ELM models.

In the prediction results of the test set, the absolute error distribution of the prediction results of tensile strength, yield strength, and elongation in different models is shown in Figure 12. As shown in Figure 12(a), the prediction error range of tensile strength in the GWO-ELM model is smaller than that of the other two models. As shown in Figure 12(b), the prediction error range of yield strength on the GWO-ELM model is smaller than that of the other two models. As shown in

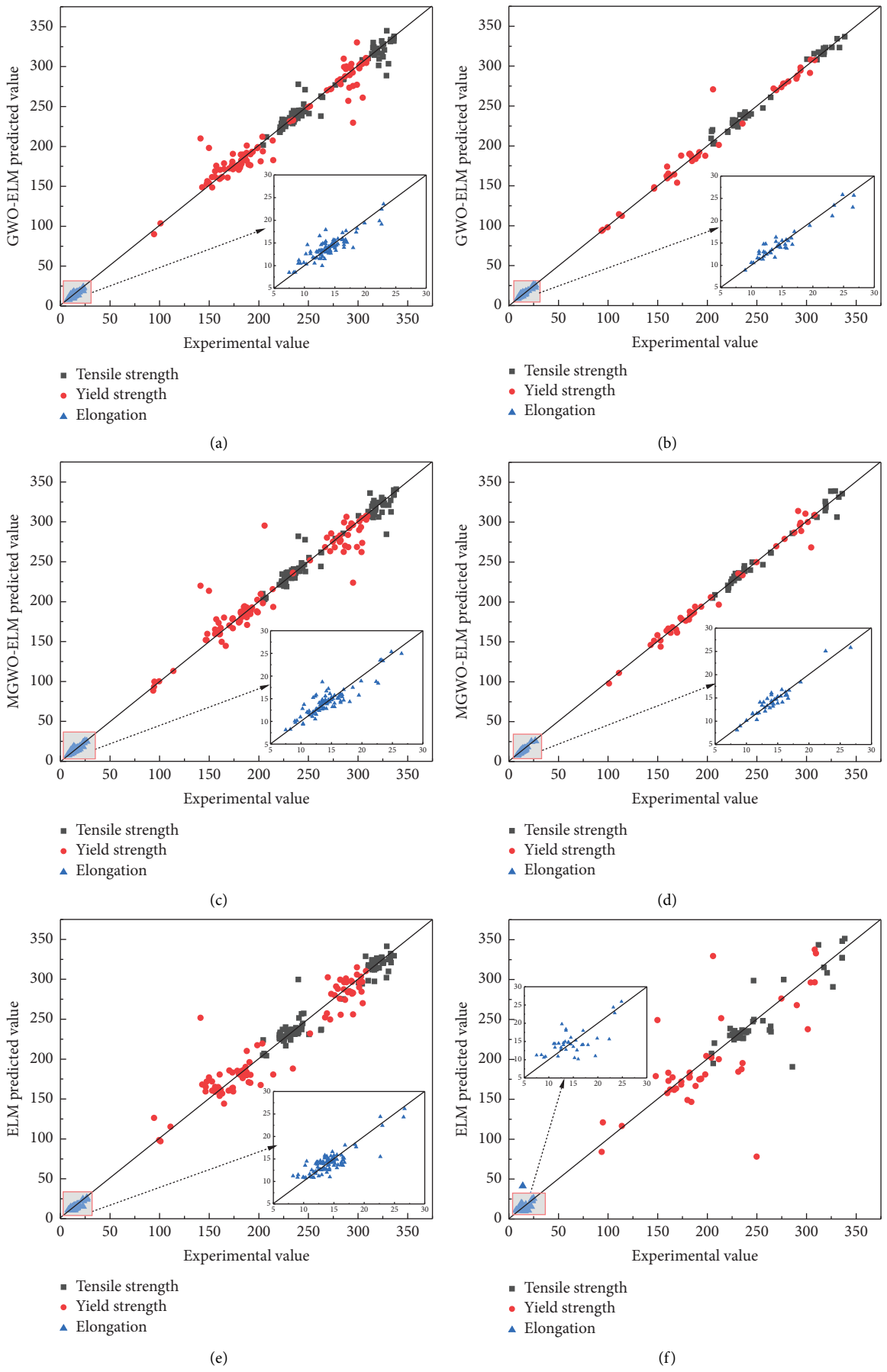

Figure 11: Predicted versus actual values of the (a) GWO-ELM training set, (b) GWO-ELM test set, (c) MGWO-ELM training set, (d) MGWO-ELM test set, (e) ELM training set, and (f) ELM test set.

Table 8: Distribution of prediction errors for the three model test sets.

Mechanical properties	Name	Prediction value deviation (%) Correct ratio (%) [0, 5]	[5, 10]	[10, 15]	[15, 20] set	[20, +∞]
Tensile strength	GWO-ELM	95	5	0	0	0
	MGWO-ELM	95	2.5	0	0	2.5
	ELM	65	15	15	0	5
Yield strength	GWO-ELM	87.5	10	5	2.5	2.5
	MGWO-ELM	62.5	30	2.5	2.5	2.5
	ELM	37.5	25	7.5	7.5	22.5
Elongation	GWO-ELM	57.5	20	12.5	5	5
	MGWO-ELM	42.5	25	10	7.5	15
	ELM	12.5	25	7.5	15	40

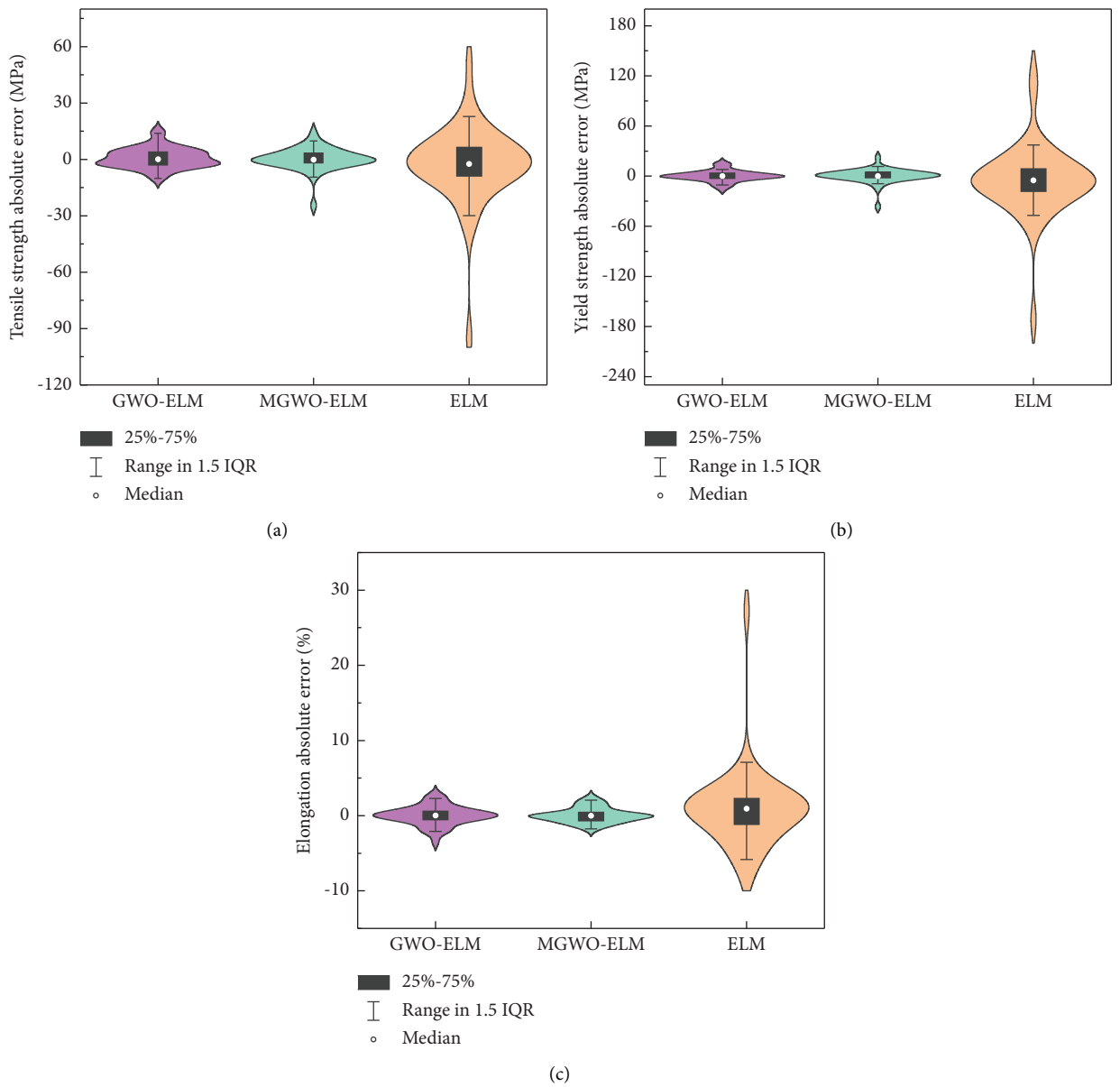

Figure 12: Absolute error distribution of the mechanical properties: (a) tensile strength, (b) yield strength, and (c) elongation.

Figure 12(b), the prediction error range of yield strength in the GWO-ELM model is significantly smaller than that of the other two models. The GWO-ELM model performs better than the MGWO-ELM model in predicting tensile strength and yield strength but not in predicting elongation. As shown in Figure 12(c), the MGWO-ELM model is slightly better than the GWO-ELM model in the prediction of elongation. In general, compared with the other two models, the prediction accuracy of tensile strength, yield strength, and elongation can be higher in the GWO-ELM model.

5. Conclusion

This paper proposes an intelligent optimization algorithm, which has the advantages of a simple structure, short training time, and high prediction accuracy. This algorithm is successfully applied to the prediction of mechanical properties of aluminium alloy strips in this paper and eventually achieves high prediction accuracy, providing a new method for predicting the mechanical properties of aluminium alloy strips, which has broad application prospects.

(1) Preprocessed industrial production data were used to train and test the GWO-ELM model. Through several experiments, the optimal network structure of the ELM algorithm and the optimal parameters of the Grey Wolf algorithm were determined. The weights and biases of the ELM were determined by the GWO algorithm. The optimal GWO-ELM model structure was successfully determined.

(2) After repeated training, the RMSEs of the GWO-ELM model for tensile strength, yield strength, and elongation were 5.365, 11.881, and 1.268, respectively. While the corresponding RMSEs of the MGWO-ELM model were 11.557, 20.465, and 1.845, and the corresponding RMSEs of the ELM model were 21.489 and 43.313. This indicates that the ELM model optimized by the GWO algorithm has higher prediction accuracy.

(3) When the prediction deviation is controlled within ±10%, the prediction accuracy of tensile strength in the GWO-ELM model, MGWO-ELM model, and ELM model is 100%, 97.5%, and 80%, respectively. The prediction accuracy of yield strength of the GWO-ELM model, MGWO-ELM model, and ELM model is 97.5%, 92.5%, and 62.5%, respectively. The prediction accuracy of elongation in the GWO-ELM model, MGWO-ELM model, and ELM model is 77.5%, 77.5%, and 37.5%, respectively. The comprehensive performance of the GWO-ELM model in predicting tensile strength, yield strength, and elongation is better than that of the other two models. The GWO algorithm successfully improves the stability and robustness of the ELM model.

Data Availability

The data used to support the findings of this study are available from the corresponding author upon request.

Conflicts of Interest

All authors declare that they have no conflicts of interest.

Acknowledgments

This work was supported by the Major Project of Science and Technology in Nanning (No. 20191002).

References

[1] G. Maizza, R. Pero, M. Richetta, and R. Montanari, "Continuous dynamic recrystallization (CDRX) model for aluminum alloys," *Journal of Materials Science*, vol. 53, no. 6, pp. 4563–4573, 2018.

[2] X. Li, M. Xu, and Z. Zhang, "Hot Damage Evolution in a High Strength Aluminum alloy during Hot Forming," *A Study Using the Gurson Journal of Materials Research and Technology*, vol. 14, 2021.

[3] D. Diehl, C. Kohler, E. L. Schneider, and T. G. R. Clarke, "Eddy current at high temperatures for in-situ control of heat treatment precipitation in hardening aluminum alloys," *IEEE Sensors Journal*, vol. 20, no. 23, pp. 14514–14520, 2020.

[4] C. H. Jia, C. X. Liu, Y. C. Liu, C. Li, and H. J. Li, "Microstructural evolution and constitutive models of 9CrMoCoB heat-resistant steel during high-temperature deformation," *Journal of Iron and Steel Research International*, vol. 26, pp. 1228–1239, 2019.

[5] H. Zhang, G. Chen, Q. Chen, F. Han, and Z. Zhao, "A physically-based constitutive modelling of a high strength aluminum alloy at hot working conditions," *Journal of Alloys and Compounds*, vol. 743, pp. 283–293, 2018.

[6] M. C. Karthik Rao, L. Malghan Rashmi, F. Kara, S. Arunkumar, S. Rao Shrikantha, and A. Herbert Mervin, "Influence of support vector regression (SVR) on cryogenic face milling," *Advances in Materials Science and Engineering*, vol. 2021, Article ID 9984369, 18 pages, 2021.

[7] G. Pilania, "Machine learning in materials science: from explainable predictions to autonomous design," *Computational Materials Science*, vol. 193, Article ID 110360, 2021.

[8] S. Guo, J. Yu, X. Liu, C. Wang, and Q. Jiang, "A predicting model for properties of steel using the industrial big data based on machine learning," *Computational Materials Science*, vol. 160, pp. 95–104, 2019.

[9] Q. Zou, L. Chen, N. Xiong, S. Zou, and C. Wang, "Prediction and Key Computer Programming of Mechanical Properties of Hot Rolled Plate Based on BP Neural Network," in *Proceedings of the 2009 International Conference on Computational Science and Engineering*, Vancouver, BC, Canada, Auguest 2009.

[10] M. Hu, Q. Tan, R. Knibbe et al., "Prediction of mechanical properties of wrought aluminium alloys using feature engineering assisted machine learning approach," *Metallurgical and Materials Transactions A*, vol. 52, no. 7, pp. 2873–2884, 2021.

[11] N. Lenzen and O. Altay, "Machine learning enhanced dynamic response modelling of superelastic shape memory alloy wires," *Materials*, vol. 15, no. 1, p. 304, 2022.

[12] Q. Lan, X. Wang, J. Sun et al., "Artificial neural network approach for mechanical properties prediction of as-cast A380 aluminum alloy," *Materials Today Communications*, vol. 31, Article ID 103301, 2022.

[13] C. Wu, C. Wang, and J. W. Kim, "Bending deformation prediction in a welded square thin-walled aluminum alloy

tube structure using an artificial neural network," *The International Journal of Advanced Manufacturing Technology*, vol. 117, no. 9-10, pp. 2791–2805, 2021.

[14] R. Jaafreh, U. M. Chaudry, K. Hamad, and T. Abuhmed, "Age-hardening behavior guided by the multi-objective evolutionary algorithm and machine learning," *Journal of Alloys and Compounds*, vol. 893, Article ID 162104, 2022.

[15] Y. Sun, W. Zeng, Y. Han et al., "Determination of the influence of processing parameters on the mechanical properties of the Ti-6Al-4V alloy using an artificial neural network," *Computational Materials Science*, vol. 60, pp. 239–244, 2012.

[16] E. Aykut, A. A. Elmas, and A. Mustafa, "Artificial intelligence-based surface roughness estimation modelling for milling of AA6061 alloy," *Advances in Materials Science and Engineering*, vol. 2021, p. 10, 2021.

[17] F. Kara, M. Karabatak, M. Ayyıldız, and E. Nas, "Effect of machinability, microstructure and hardness of deep cryogenic treatment in hard turning of AISI D2 steel with ceramic cutting," *Journal of Materials Research and Technology*, vol. 9, no. 1, pp. 969–983, 2020.

[18] I. V. Manoj, S. Hargovind, S. Narendranath, P. M. Mashinini, and F.. Kara, "Examination of machining parameters and prediction of cutting velocity and surface roughness using RSM and ANN using WEDM of altemp HX," *Advances in Materials Science and Engineering*, vol. 2022, Article ID 5192981, 9 pages, 2022.

[19] G. B. Huang, Q. Y. Zhu, and C. K. Siew, "Extreme Learning Machine: Theory and Applications," *Neurocomputing*, vol. 70, no. 1, 2005.

[20] Z. Cao, J. Xia, M. Zhang et al., "Optimization of gear blank preforms based on a new R- GPLVM model utilizing GA-ELM," *Knowledge-Based Systems*, vol. 83, 2015.

[21] X. Sui and Z. Lv, "Prediction of the mechanical properties of hot rolling products by using attribute reduction ELM," *The International Journal of Advanced Manufacturing Technology*, vol. 85, no. 5-8, 2016.

[22] J. Liu, X. Liu, and T. Le, "Rolling Force Prediction of Hot Rolling Based on GA-MELM," *Complexity*, vol. 2019, Article ID 3476521, 11 pages, 2019.

[23] H. Faris, I. Aljarah, M. A. Al-Betar, and S. Mirjalili, "Grey Wolf Optimizer: A Review of Recent Variants and Applications," *Neural Computing and Applications*, vol. 30, no. 22, 2018.

[24] Y. Zhang and X. Zhou, "An Improved Grey Wolf Algorithm for Solving Global Optimization Problems," *Journal of University of Shanghai for Science and Technology*, vol. 166, no. 01, pp. 73–82, 2021.

[25] L. Rodríguez, O. Castillo, J. Soria, and J. Soto, "A fuzzy hierarchical operator in the grey wolf optimizer algorithm," *Applied Soft Computing*, vol. 57, 2017.

[26] S. Saremi and Seyedeh Zahra Mirjalili & Seyed Mohammad Mirjalili, "Evolutionary population dynamics and grey wolf optimizer," *Neural Computing and Applications*, vol. 26, no. 5, 2015.

[27] M. Mengcan, C. Xiaofang, and X. Yongfang, "Constrained voting extreme learning machine and its application," *Journal of Systems Engineering and Electronics*, vol. 32, 2021.

[28] S. Wu, G. Cao, X. Zhou, N. Shi, and Z. Liu, "High dimensional data-driven optimal design for hot strip rolling of C-Mn steels," *ISIJ International*, vol. 57, pp. 1213–1220, 2017.

[29] P. Y. Chou, J. T. Tsai, and Jyh-Horng Chou, "Modeling and optimizing tensile strength and yield point on a steel bar using an artificial neural network with taguchi particle swarm optimizer," *IEEE Access*, vol. 4, 2016.

[30] Ö. Erkan, B. Işık, A. Çiçek, and F. Kara, "Prediction of damage factor in end milling of glass fibre reinforced plastic composites using artificial neural network," *Applied Composite Materials*, vol. 20, no. 4, pp. 517–536, 2013.